ELSEVIER

Contents lists available at ScienceDirect

Materials Today Physics

journal homepage: www.journals.elsevier.com/materials-today-physics





Lead-free bismuth pyrochlore-based dielectric films for ultrahigh energy storage capacitors

Sung Sik Won a , Hyunseung Kim b,c , Jinkee Lee d , Chang Kyu Jeong b,c,* , Seung-Hyun Kim a,** , Angus I. Kingon a

- a School of Engineering, Brown University, Providence, RI, 02912, United States
- ^b Division of Advanced Materials Engineering, Jeonbuk National University, Jeonju, Jeonbuk, 54896, South Korea
- ^c Department of Energy Storage/Conversion Engineering of Graduate School & Hydrogen and Fuel Cell Research Center, Jeonbuk National University, Jeonju, Jeonbuk, 54896. South Korea
- ^d School of Mechanical Engineering, Sungkyunkwan University, Suwon, Gyeonggi, 16419, Republic of Korea

ARTICLE INFO

Keywords: Lead-free Pyrochlore dielectrics Film capacitor Pseudo-linearity Chemical solution deposition

ABSTRACT

We developed ultra-high energy storage density capacitors using a new class of lead-free bismuth pyrochlore-based dielectric film material systems with high breakdown strength and reliability. The 2 μ m-thick pyrochlore ceramic film capacitors have demonstrated ultra-high energy densities around 90 J/cm³ with very low energy loss below 3%, which is achieved by the combination of high permittivity, pseudo-linear dielectric characteristics, and high breakdown electric field over 4.5 MV/cm. Particularly, these pyrochlore ceramic films can endure voltage strength up to ~900 V. These noteworthy pyrochlore ceramic films are fabricated by the low-cost chemical solution deposition process which allows dielectric films to be processed on standard platinized silicon wafers. This new class of capacitors can satisfy the emergent needs for significant reduction in size and weight of capacitors with high energy storage capability in power electronics, electric vehicles, and energy storage in sustainable energy systems. Our research provides a unique and economical platform for the processing of this useful pyrochlore material in large volume for eco-friendly energy applications.

1. Introduction

According to the rapid expansion of power electronics in multiple applications such as electric vehicles, energy distribution, space systems, medical devices, military weapon systems and other commercial applications, there is a concomitant demand for high energy storage and supply systems such as batteries, electrochemical supercapacitors and dielectric capacitors [1–6]. Even though rechargeable batteries are most widely used in current energy storage and supply systems, these have various limitations such as restricted useable temperature range, over-current and electrical shock, slow charging and discharging time (i. e. limited power density), etc. Therefore, it is required that batteries are complemented with capacitors for many systems which need high power density [7–9]. Recent studies have significantly focused on the so-called supercapacitors or ultracapacitors (i.e. electrochemical capacitors), but they suffer from inevitably restricted low-voltage operation (i.e. ~3 V), which makes their volumetric energy storage density very low.

Furthermore, they present limited cycle life ($\sim 10^6$ cycles), and relatively high leakage current (~microamperes) [3,10-12]. These problems virtually eliminate the usefulness of supercapacitors from high-voltage power-electronic applications such as electric vehicle applications [1,10,13]. On the contrary, dielectric capacitors can exhibit very high power density and deliver large amount of energy within very short time from milliseconds to microseconds, which generates intense pulsed voltage or current [2,14]. In addition to the high power density and fast charging-discharging process, dielectric capacitors can be operated at much higher input voltage with longer lifetime and higher thermal stability than electrochemical supercapacitors and batteries. Such unique characteristics make dielectric capacitors promising candidates for energy storage systems in many pulsed power conditioning electronic applications. Nevertheless, there are still well-recognized demands for high-performance dielectric capacitors, sparking an ongoing need to identify and develop new dielectric materials with improved energy storage density and reliability. Namely, significant

E-mail addresses: ckyu@jbnu.ac.kr (C.K. Jeong), seunghyun_kim@brown.edu (S.-H. Kim).

^{*} Corresponding author. Division of Advanced Materials Engineering, Jeonbuk National University, Jeonju, Jeonbuk, 54896, South Korea.

^{**} Corresponding author.

studies are required for improved combinations of sufficient dielectric breakdown strength, high dielectric constant with low dielectric loss, and high thermal stability with minimal thermal runaway, while at the same time avoiding the toxicity of common Pb-based dielectric ceramics. In addition to developing high energy density dielectric materials, the energy storage capacitors integrated into current power electronic systems need significant size-scale reduction so that power conditioning modules of increasing capacity and functionality can be incorporated into a great range of device applications [2,14]. Therefore, film-type high-energy density capacitors with strong durability and reliability are of importance for the successful deployment of envisaged energy storage systems in current pulsed power circuits.

Recently, cubic phase-based pyrochlore dielectric ceramics with slimmer hysteresis loops and lower energy losses than those of ferroelectric or antiferroelectric materials have shown promise for highperformance energy storage applications [15–17]. As a member of the pyrochlore family, the non-ferroelectric bismuth zinc niobate (Bi-Zn-Nb-O, BZN)-based materials have been of particular interest to energy storage capacitors because they are typical pseudo-linear dielectric materials with high breakdown strength, low dielectric loss and high thermal stability up to 150-200 °C which is the general working temperature of the engine of electrical vehicles [15-19]. Stoichiometric pyrochlores have the general formula of A₂B₂O₇ (where A is trivalent or bivalent cations and B is quadrivalent or quinquevalent cations) [16-19]. The structure is composed of two different types of cation coordination polyhedrons; the A-site positions eight-coordinate and are typically occupied by larger cations, while smaller sized cations favor the six-coordinate B-site positions. Interestingly, Zn ions can occupy both A- and B-sites in BZN-based pyrochlore dielectric ceramics, resulting in diverse structures with a wide range of different chemical substituents. In general, however, this material system exhibits a low dielectric constant around 100 even with a low maximum polarization (~20 μC/cm²) after excluding leakage current contributions at maximum electric fields [16-19]. To resolve these drawbacks, we have designed BZTN using the addition of Ti cation into the pure BZN [i.e., $(Bi_{1.5}Zn_{0.5})$ $(Zn_{0.5}Nb_{1.5})O_7$] film to improve the dielectric properties, especially for increasing the permittivity and reducing the dielectric loss with the original advantages of BZN materials.

In this study, we thoroughly investigate the material properties of Tidoped BZN (BZTN) lead-free ceramic films and address their potential to achieve high voltage stable and high energy storage capable film capacitors, utilizing the cost-effective and scalable chemical solution processes. The film capacitor shows ultra-high energy storage density with low loss and high breakdown strength; the 2 μ m-thick ceramic film can be operated at very high voltage up to $\sim\!900$ V. Based on basic and engineering science, we propose to bring several innovations to the development of specific BZTN for investigating the principle and performance of this material to meet the rapidly increasing industry demands.

2. Experimental

2.1. Synthesis of BZN and BZTN chemical solutions and related film deposition

For lead-free film-based energy storage capacitors, Bi-based pyrochlore (Bi_{1.5}Zn_{0.5}) (Zn_{0.5}Nb_{1.5})O₇ (BZN) and (Bi_{1.5}Zn_{0.5}) (Ti_{1.5}Nb_{0.5})O₇ (BZTN) chemical solutions were prepared using Bi-nitrate pentahydrate [Bi(NO₃)₃·5H₂O, 99.99%], Zn-acetate dehydrate [Zn(CH₃COO)₂·2H₂O, \geq 99%], Ti-tetra-i-propoxode [Ti(O-i-CH₃H₇)₄, 99.999%] and Nbethoxide [Nb(O–C₂H₅)₅, 99.9%] as main metal precursors. These all chemicals were purchased from Kojundo Chemical Laboratory Co. Ltd. For eco-friendly regulation and environmental compatibility, we chose non-toxic butanol (>99.4%, Sigma-Aldrich) as a reactant and solvent instead of toxic 2-methoxyethanol. To prepare stable solutions, we used

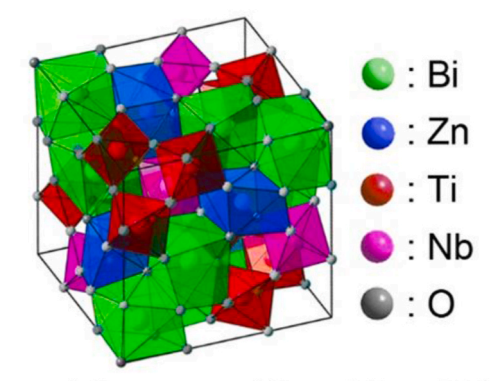
acetylacetone (>99%, Sigma-Aldrich) as a chelating agent for the solutions to reduce the hydrolysis reactivity and the condensation reactions. Besides chelating effects, the acetylacetone could enhance the solubility of precursors in the solution. The synthesized Bi-based solutions were spin-casted onto Pt (150 nm)/Ti (10 nm)/SiO2 (300 nm)deposited Si wafers at 3000 rpm for 30 s. Then, it was subsequently dried at 450 °C for 7 min and annealed at 650 °C for 3 min for each layer. The thickness of each BZN or BZTN layer was 100 nm. The final film thickness was measured to be about 2 μm observed by the SEM. After all of the layers were deposited, the coated ceramic films were crystallized at 650 °C for 30 min in a pre-heated tube furnace. Fig. S2 shows the detailed process diagram about the fabrication of our Bi-based pyrochlore films. The Pt thin film was deposited upon the BZN or BZTN film as circular top electrodes with the diameter of ${\sim}200~\mu m$ and the thickness of \sim 150 nm by a sputtering system (Kurt J. Lesker Company) and subsequently annealed at 650 °C for 15 min to relax the plasma damage from the sputtering system. Note that the size of top electrodes was defined using an optical microscope for the accurate characterization of electrical properties of the ceramic films.

2.2. Characterization

The structural and crystallographic characterizations of BZN and BZTN films were investigated by using an X-ray diffraction (XRD, Bruker Corporation, Billerica, USA) with Cu K α radiation (the wavelength of 1.54 Å). The top-view surface and cross-sectional images of the films were specified by a field emission scanning electron microscopy (FE-SEM, JEOL JSM-6700 F and Carl Zeiss Gemini500). Some SEM images were analyzed in the Center for University-wide Research Facilities (CURF) at Jeonbuk National University. The dielectric constant and tangent loss of the films were measured by an impedance analyzer (HP4294A). The *P-E* loops were determined by the Precision Premier II ferroelectric tester (Radiant Technologies, Albuquerque, USA) with a high voltage amplifier available up to 10 kV (TREK Inc., USA). The leakage current density of both films was measured as a function of applied voltages up to 400 V using a DC current test equipment (Keithley 2470 high voltage source meter, USA).

3. Results and discussion

Fig. 1 shows the crystal structure of pyrochlore BZTN [i.e., $(Bi_{1.5}Zn_{0.5})$ $(Zn_{0.5-x/3}Ti_xNb_{1.5-2x/3})O_7]$ and its dielectric properties as a function of Ti composition in BZTN films. Dielectric constant of BZTN pyrochlore films increases from ~100 to ~270 with increasing the composition of Ti from 0 to 1.5 mol %. All compositions present low dielectric loss around the order of 0.001-0.002 at the frequency of 1 kHz. In the BZTN pyrochlores, the high dielectric constant is provided by the structures with BO₆ octahedra joined and linked each other by their tops in the A₂B₂O₇ pyrochlore phase [20-22]. Considering the radius and valence of cations, it could be assumed that Ti⁴⁺ can co-substitute ${\rm Zn}^{2+}$ and ${\rm Nb}^{5+}$ at the B-sites. The ionic radius of ${\rm Zn}^{2+}$, ${\rm Nb}^{5+}$ and ${\rm Ti}^{4+}$ with eight-coordination number is 0.75, 0.64 and 0.61 Å, respectively. The mechanism of substitution can be expressed as the following Kröger-Vink notation: $3Ti_{Ti}^{\times} \to Ti_{Zn}^{-} + \ 2Ti_{Nb}^{'}$. Therefore, the criterion of charge neutrality can also be satisfied. In addition, Valant et al. demonstrated that the lattice parameters of the solid solutions decrease with increasing the Ti concentration up to 1.5 mol% (10.55 for 0 mol% of Ti and 10.35 for 1.5 mol% of Ti substitution), and a discontinuity of cell volumes in this variation is apparent at 1.5 mol% of Ti, where the Zn cations on the B-site positions are completely substituted by Ti cations [23]. The composition of this solid solution can be represented as $(Bi_{1.5}Zn_{0.5})$ $(Ti_{1.5}Nb_{0.5})O_7$. Therefore, the key B-site cations located in the center of octahedra are Ti⁴⁺, Zn²⁺ and Nb⁵⁺ below the 1.5 mol% of Ti, whereas Ti⁴⁺ and Nb⁵⁺ at 1.5 mol% of Ti. Consequently, it is reasonable that the Ti cations are expected to initially substitute both



Crystal Structure of Pyrochlore BZTN

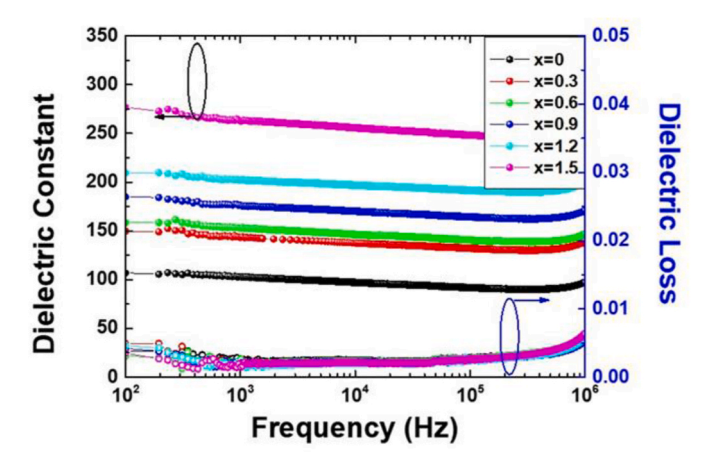


Fig. 1. (Top) Crystal structure of BZTN pyrochlore. (bottom) Measurement of dielectric constant (relative permittivity) of (Bi_{1·5}Zn_{0.5}) (Zn_{0.5·x/3}Ti_xNb_{1.5·2x/3}) O_7 (BZTN) films as a function of Ti doping concentration. Dielectric constant of pyrochlore BZTN films increases from 100 to 270 with increasing the Ti concentration from 0 to 1.5 mol %. All films show low loss tangents on the order of 0.001–0.002 at the frequency of 1 kHz, regardless of the Ti doping concentration.

 ${\rm Zn^{2+}}$ and ${\rm Nb^{5+}}$ cations that are located on the B-sites of the pyrochlore structure and composition. There is a strong correlation between highly polarizable octahedra of ${\rm TiO_6}$ and ${\rm NbO_6}$, which causes the high dielectric constant for the Ti-rich region, as shown in Fig. 1. According to the result, we selected the Ti composition of 1.5 mol% in the BZTN films for high energy storage capacitor applications.

Because the cubic BZTN pyrochlore films can possess high dielectric constant and maximum polarization, it is an optimal choice for film capacitors if sufficient thickness (a few µm) can be formed. Note that recent studies have reported that maximum energy storage density is not only obtained just by high dielectric constant, but also by the highest applicable ultimate breakdown electric field and voltage even with intermediate dielectric constant [15-17]. The electrical breakdown strength mainly depends on microstructure and thickness of dielectric films, so the reasonable film thickness with high thickness/volume ratio is important. Unfortunately, most reported pyrochlore films with the cubic phase have shown the limited thickness formation below 300 nm because of high internal stress, related cracks, and serious delamination in the films during certain processes, which results in very low breakdown voltage strength by the low thickness/volume ratio, although the electric field strength can be calculated high [15-19]. In the chemical solution deposition (CSD) method of lead-free BZN-based films, large volume changes during the firing process induce high internal stress within the film, which can cause mechanical cracks or delamination of the film. It can be more severe by multiple pyrolysis processes to

increase the film thickness (Fig. S1). To achieve crack-free BZTN films even with µm-scale thickness, a sophisticated control of drying and pyrolysis processes is essential to completely eliminate the organic residues and relax the internal stress in the film. The low-temperature drying process below 350 °C induces serious cracks and delamination of BZTN thin films with increasing film thickness due to the incomplete removal of residual organics and the built-up internal stress within the film. To prevent the mechanical failures of films, we demonstrated the two-step drying and pyrolysis processes for each deposited layer at relatively high temperature, as shown in the details of Experimental Section and Fig. S2. The complete pyrolysis of organometallic compounds and the partial crystallization of each layer with this multiple firing method could effectively prevent any cracks and provide dense microstructure with homogeneous nanoscale grain size of the films even after the final annealing step of whole thickness at 650 °C for 30 min. Fig. 2a and b shows scanning electron microscopy (SEM) images of pure BZN and 1.5 mol% Ti-contained BZTN films, respectively. Both films present similar feature of surfaces, indicating highly dense and uniform microstructures without any visible pores. In addition to highly dense and uniform microstructures, small grain size (large area of grain boundary) is also important to reduce the leakage current density and enhance the breakdown strength of dielectric films because the conductivity of grain boundary is generally much lower than grain interior in most oxide dielectric materials, resulting in high breakdown strength and thus high energy storage density [14,24,25]. The average grain size of the BZN and BZTN films is around 15-20 nm, which is much smaller than that of most µm-thick ferroelectric or antiferroelectric films showing the general grain size of 100–300 nm [22,26–29].

The key question for utilizing film dielectric materials instead of bulk ceramics is whether these materials can compete in the race for downscaling with highly adaptable and reliable properties. As materials become thinner, the classical dielectric characteristics may be changed by certain conditions such as serious leakage current, low breakdown strength and easy degradation, which need to be addressed. Recently, some studies reported ultrahigh energy storage density of dielectric film capacitors using very thin polycrystalline or epitaxial films because of the high electric field strength according to reducing thickness [30–34]. However, many practical capacitor applications require high operation voltages over several hundred volts, beyond just high electric fields. In addition, it should be noted that the total absolute energy storage capacity of ultra-thin film-based capacitors is too small due to its low thickness/volume ratio, which are not suitable for practical applications. This industrial request implies that the dielectric films should endure very high voltage with adequate thickness [2,15,35,36]. Fig. 2c shows the cross-sectional SEM image of our BZTN film, which indicates dense morphology as well as clean interface between the film and the substrate. The thickness of crack-free BZTN film is 2 μm suitable for practical film capacitors. Fig. 2d presents the X-ray diffraction (XRD) patterns of pure BZN and BZTN films, respectively. Both films have the pure pyrochlore phase with randomized, but relatively (222)-preferred orientation without secondary phases. The activation energy for the nucleation of BZN-based thin films is the lowest in the case of heterogeneous nucleation on lattice-matched substrates, which implies that the films on Pt (111) substrates generally show a highly textured (222) orientation. Nevertheless, it should be noted that the intrinsically lowest activation energy of the growth plane of the BZN-based films is dwell in the (200) plane. Therefore, the accidental arising (200)-oriented nuclei of the films tend to grow more rapidly than other orientations. This is the main reason why the films have either (222)-preferred or (222)/(200)-mixed preferred orientation on (111) Pt substrates. Note that (200) is finally shown as the (400) peak. In addition, if there is strong competition between the activation energy for nucleation and growth of the films during the crystallization process, sometimes it leads to other randomized orientations including the (440) direction. It should be mentioned that (440) is one of main peaks in the XRD of the bulk sintered ceramics without any specifically oriented substrates.

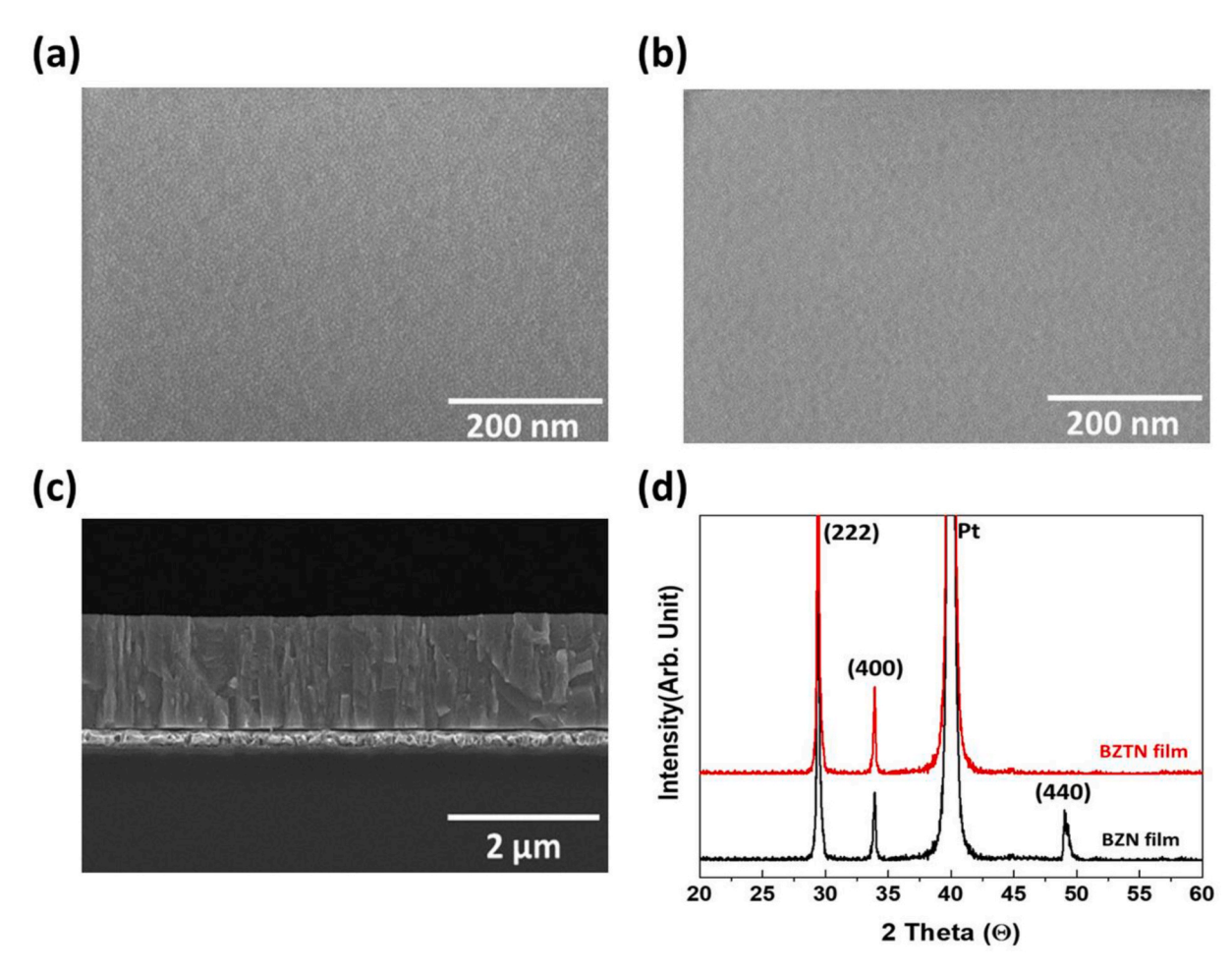


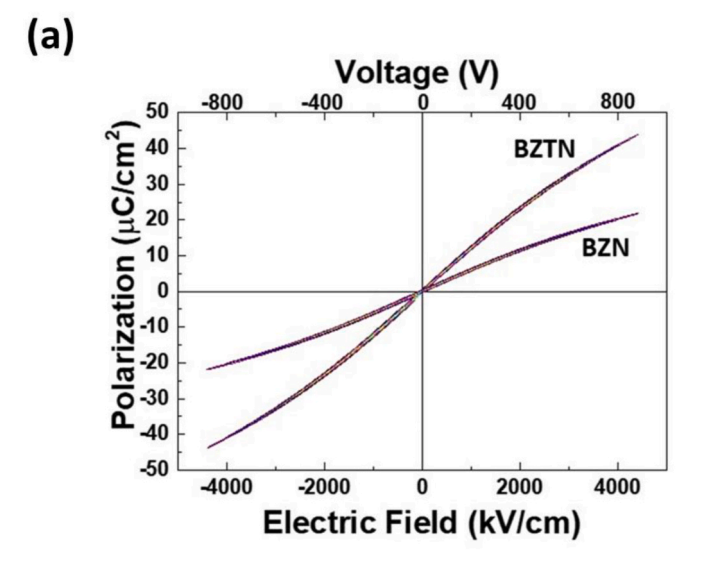
Fig. 2. SEM surface images of (a) pure BZN and (b) 1.5 mol% Ti-doped BZTN ceramic films, which represents highly dense and uniform microstructures without any visible pores. The average grain size of both films is around 15–20 nm. (c) Cross-sectional SEM image of the BZTN film. The thickness of the film is about 2 µm. (d) XRD patterns of the pure BZN and the BZTN films. Both films have a pure pyrochlore phase with the randomized, but relatively (222)-preferred orientation.

Therefore, the (440) orientation of the films is minor and may or may not appear during the process. It is obvious that there is the preferred orientation of films on the Pt substrates, which does not affect the properties of the BZN-based films.

Fig. 3a shows typical polarization (P) - electric field (E) hysteresis curves of 2 µm-thick pure BZN and BZTN films, which present pseudolinear and extremely slim hysteresis behaviors even at the high electric field of 4.5 MV/cm (~900 V) without any premonition of failure. Both films have low coercive field and negligible remnant polarization because of the cubic phase-based pyrochlore crystallographic structure. In contrast, it should be mentioned that the P-E hysteresis loops of both films show huge polarization and abnormal hysteretic behaviors without saturation level at the applied electric field of 5 MV/cm (~1000 V) (Fig. S3). Such the abnormal hysteresis shape and the huge nonsaturated polarization values usually indicate large leakage currents through the films. In the case of electrical leakage and breakdown, the ferroelectric tester generally measures the leakage charges collected on the integrated capacitors and converts them to the polarization values, which means that the abnormally high polarization hysteresis behaviors like Fig. S3 are not real ferroelectric ones. Therefore, it should be considered that the shape of P-E hysteresis curves and polarization values at high electric fields could be affected by the leakage current and its tricky charges throughout the tester, which often leads to false or misleading information upon the calculation for the energy storage capacity of films. Based on these results, we can specify the maximum applied electric field of 4.5 MV/cm on both BZN and BZTN films for energy storage capacitor applications.

As shown in Fig. 3a, the BZTN film shows approximately two times higher maximum polarization than that of the pure BZN film up to the applied electric field of 4.5 MV/cm. The maximum polarization values of BZN and BZTN films are 21.8 and 43.9 $\mu\text{C/cm}^2$, respectively. As aforementioned in Fig. 1, this is presumably due to the aliovalent Ti dopant cations, which have the higher polarizability of Ti–O, resulting in the higher permittivity as well as the higher maximum polarization.

Fig. 3b shows the leakage current density of both films as a function of applied DC voltage input up to 400 V. The leakage current density of the films is not raised significantly with increasing the applied voltages over 400 V where it shows the low value around 10^{-8} A/cm². In dielectric oxides, it has been reported that resistivity of the grain boundaries is two orders of magnitude higher than the resistivity of grain interior [14,24,25]. In the SEM images of Fig. 2, both films show nanoscale grain size of 10–20 nm. Therefore, plenty of grain boundaries can impede electrical conduction through both films, resulting in low leakage current density and high breakdown strengths. It should be noted that the leakage current density of the BZTN film (9 \times 10⁻⁸ A/cm² at 400 V) is slightly higher than that of the pure BZN film (2 \times 10⁻⁸ A/cm² at 400 V). It is well known that the higher band gap of dielectric materials results in the higher breakdown strength and the lower leakage current density due to the lower electrical conduction [17]. The titanium oxide dopant exhibits the band gap of approximately 3.2-3.3 eV, while the niobium oxide host has the band gap of about 3.4 eV. Thus, it is anticipated that the higher polarizability (also resulting in the higher relative permittivity) of the Ti-O in the BZTN film may induce the slightly higher leakage current density than the pure BZN film, but the



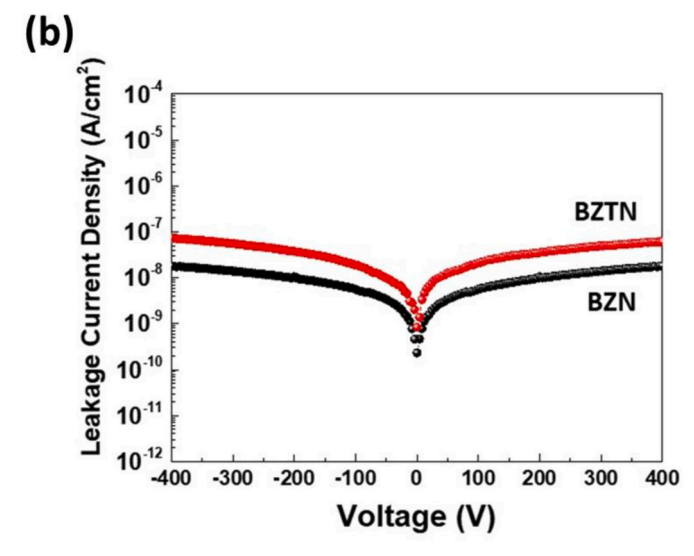


Fig. 3. (a) *P-E* hysteresis loops of pure BZN and BZTN films of 2 μ m in thickness. Both films show very slim hysteresis loops with the very low coercive field and the negligible remnant polarization. (b) Leakage current density of both films as a function of applied voltages up to 400 V. The leakage current density of the films does not increase significantly with increasing the applied voltages to 400 V and shows the low value of $\sim 10^{-8}$ A/cm².

absolute level of leakage characteristics is still low within both films.

Fig. 4a illustrates the schematics of pseudo-linear dielectric P-E hysteresis and the corresponding energy storage performance of our Bi-based pyrochlore ceramic films. Generally, the total energy storage density (Utotal) of dielectric capacitors is expressed as Equation (1).

$$U_{\text{total}} = \int EdP \tag{1}$$

The effective recoverable (discharged) energy storage density ($U_{\rm reco}$) is important because it is the releasable and useable energy density during discharging process from maximum electric field to zero field. In the P-E hysteresis, the $U_{\rm reco}$ is displayed as the integrated area outside of hysteresis. In contrast, the energy storage loss ($U_{\rm loss}$) is the integrated area inside of the hysteresis which means the difference between $U_{\rm total}$ and $U_{\rm reco}$, as represented by Equation (2).

$$U_{\rm loss} = U_{\rm total} - U_{\rm reco} \tag{2}$$

The energy conversion efficiency (η) can be expressed as following Equation (3).

$$\eta = \frac{U_{\text{reco}}}{U_{\text{total}}} \times 100 \, (\%) \tag{3}$$

Based on the above equations, an ideal dielectric film for high energy storage density capacitors should possess a high maximum polarization and a high dielectric permittivity with a low remnant polarization, a high breakdown strength and a low energy loss under high applied voltage as well as electric field. The reduction of energy loss is particularly essential to minimize the dissipation of stored energy density upon discharging processes. As aforementioned, the amount of energy loss is described as the area enclosed by a *P-E* hysteresis loop; thus, slim or non-hysteretic curves with very low or zero remnant polarization are highly preferred for high-performance energy storage capacitor applications [2,15].

Fig. 4b and c presents the energy storage density and the energy loss calculated from the P-E hysteresis loops of the 2 μ m-thick BZN and the BZTN film capacitors as a function of applied electric field up to 4.5 MV/cm (~900 V), respectively. As expected, the energy density levels of both films gradually increase with elevated electric field. At the maximum electric field of 4.5 MV/cm, the $U_{\rm total}$ of the BZN and BZTN film capacitors are 44.6 J/cm³ and 89.2 J/cm³, while the $U_{\rm reco}$ of them are 41.7 J/cm³ and 86.7 J/cm³, respectively. It is clearly observed that the $U_{\rm loss}$ of both film capacitors is very low (below 3 J/cm³) even at the maximum electric field of 4.5 MV/cm.

With the expanded applications of energy generation and storage technologies, high electric power output as well as high energy storage density are also essential as the performance of capacitors for many device applications. In high-power electronics including pulsed power devices, the release of large currents at the discharging process within very short time is highly required. However, the power density of batteries is quite low due to the slow movement of charge carriers, which restricts applications in various high-power device systems. Instead, supercapacitors may be able to offer improved power density at moderate levels, but the low mobility of ions in electrolytes is still a critical disadvantage for the charging/discharging rate (typically in order of seconds) and thus the final power output [10]. On the contrary, our dielectric capacitors provide much higher power density because of extremely high discharge speed. So, it can be a suitable energy storage system when high power delivery or uptake is essentially required. Fig. S4 shows the discharge time of our BZN and BZTN film capacitors with the 1 k Ω load resistor (R_L) of circuit. For dielectric capacitors, the stored energy is discharged to R_L . The standard discharge time (T_{90}) is denoted as the time for discharged energy into R_I to reach 90% of the saturated U_{reco} value, which can be obtained directly from the discharge profile. The measurement of discharging is conducted at the electric field of 4.5 MV/cm to prevent electrical breakdown or leakage current hindrance. From the discharge profile, the T_{90} for both film capacitors are similar (1.48 and 1.51 µs for the BZN and BZTN films, respectively), which demonstrates that the stored energy can be discharged within very short time (~a few μs). This standard discharging time is comparable to that of most Pb-based ferroelectric or antiferroelectric films and much faster than that of supercapacitors or batteries (mins-hrs).

Fig. 4d exhibits the charge-discharge efficiency η , which is defined as the ratio of recoverable effective energy storage density with respect to the total input energy storage density, as aforementioned Equation (3). Both BZN and BZTN ceramic film capacitors show excellent energy storage efficiency levels which are over 95%, regardless of the applied electric fields up to 4.5 MV/cm. In particular, the energy efficiency of BZTN film capacitor shows the considerably high value of 98.6% at the electric field of 2.5 MV/cm and 97.2% even at the maximum electric field of 4.5 MV/cm without notable degradation and failure. To place these results in context, it should be noted that the best Li-ion batteries have the charge/discharge efficiency around 90%, and that of some supercapacitors has been reported as up to 95% [37–39]. Moreover, the energy efficiency above 95% is very rare in the field of dielectric film capacitors [40]. Therefore, our result is extremely encouraging that the

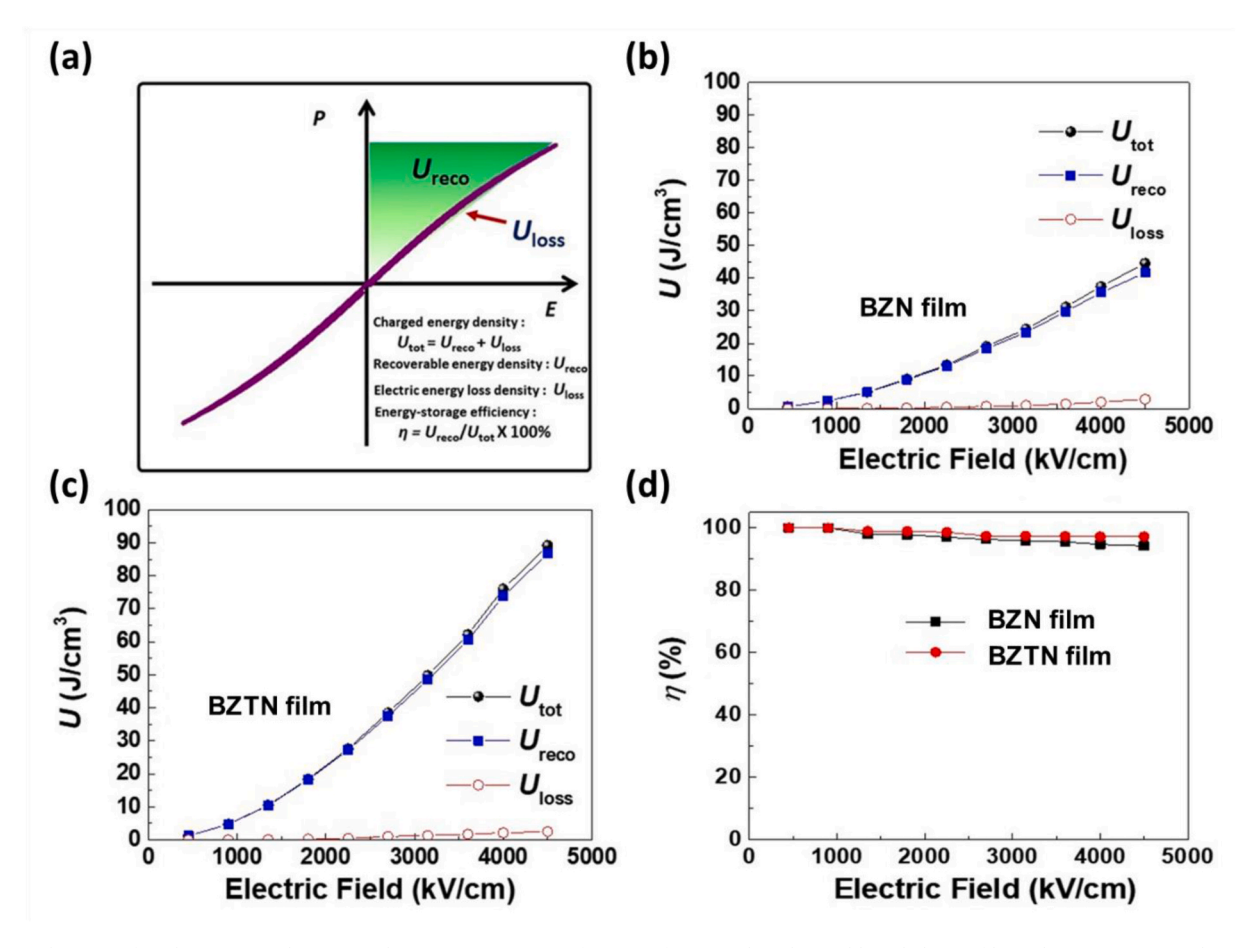


Fig. 4. (a) Schematic of *P-E* hysteresis and corresponding energy storage performance for our Bi-based pyrochlore dielectric films. The energy storage density and the energy loss calculated from *P-E* hysteresis loops of 2 μm-thick (b) BZN and (c) BZTN film capacitors as a function of applied electric field up to 4.5 MV/cm (\sim 900 V). (d) Charge-discharge efficiency (η, energy conversion efficiency) defined as the ratio of recoverable effective energy storage density with respect to the total input energy storage density.

efficiency higher than 97% is achievable even at the harsh condition around the high electric field of 4.5~MV/cm (the absolute voltage of 900 V).

Fig. 5 presents the performance of our BZTN ceramic film capacitor compared to previously reported other ceramic film capacitors to show superiority in terms of energy storage efficiency, energy storage density and absolute endurable (breakdown) voltage [14,30,31,41-71]. Particularly, high maximum endurable voltage is very difficult to accomplish while high maximum electric field can be easily obtained in the case of thin films even with the low absolute voltage input. Note that the high absolute endurable voltage is crucial to operate high-power and high-voltage electric applications. In the case of electric vehicles (EVs), for example, the dissipated energy is a big problem; Li-ion batteries run hot, so cooling is the major concern. For the application in regenerative braking, which involves rapid and repeated charge-discharge cycling, the 95% efficiency of supercapacitors is also considered problematic, so the efficiency higher than 95% has been considered as the target of state-of-the-art research. In this regard, our BZTN pyrochlore-based ceramic film shows excellent performance according to the maximum applicable voltage as well as the energy efficiency and the energy storage density. As shown in Table S1, it is definitely explained that thinner dielectric films can show higher breakdown field, but cannot have high endurable breakdown voltage in actual electrical input. Consequently, our BZTN film capacitor has been developed by the facile solution process with sufficient thickness and excellent performance, from actual breakdown voltage to energy efficiency.

4. Conclusions

To summarize, this research has systematically investigated the cubic pyrochlore phase-based BZN and BZTN films with the dielectric pseudo-linearity and demonstrated performance of thin film-type energy storage capacitors. By the facile and optimal solution process, our lead-free ceramic films have shown very dense and uniform microstructure with 2 μm in thickness and nanoscale grain morphologies which are desirable to enhance the breakdown electric field and voltage strength of the capacitors. In particular, the 1.5 mol% Ti-doped BZN for BZTN films have presented not only the highest energy storage density and the highest dielectric constant but also the highest energy conversion efficiency. The energy efficiency of the BZTN film capacitor is 98.6% at the electric field of 2.5 MV/cm (500 V) and 97.2% even at the maximum electric field of 4.5 MV/cm (900 V) without notable degradation and breakdown. The performance of our environmentallyfriendly Bi-based pseudo-linear dielectric film capacitors is extremely encouraging for high energy storage density and fast discharging power electronic applications, fully covering the important area where neither conventional supercapacitors nor Li-ion batteries can do.

Credit author statement

Sung Sik Won: Methodology, Formal analysis, Investigation, Resources. Hyunseung Kim: Investigation, Data curation, Visualization. Jinkee Lee: Validation, Funding acquisition. Chang Kyu Jeong: Conceptualization, Validation, Data curation, Writing - Original Draft, Writing - Review & Editing, Visualization, Supervision, Funding

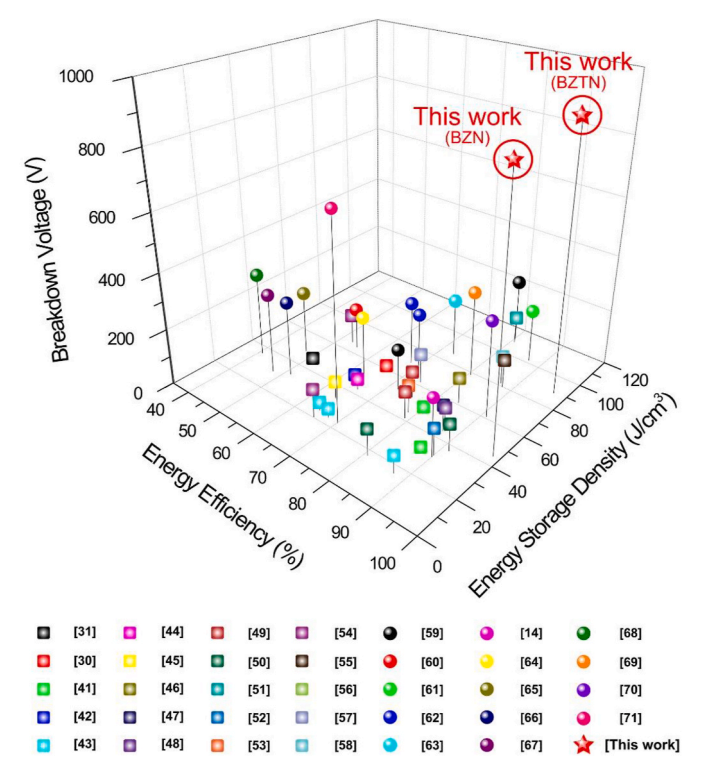


Fig. 5. Plot to show the superiority of BZT and BZTN film capacitors in this work, compared to previous reports.

acquisition. **Seung-Hyun Kim**: Conceptualization, Methodology, Validation, Resources, Data curation, Writing - Original Draft, Writing - Review & Editing, Supervision, Project administration, Funding acquisition. **Angus I. Kingon:** Validation, Project administration, Funding acquisition.

Declaration of competing interest

The authors declare that they have no known competing financial interests or personal relationships that could have appeared to influence the work reported in this paper.

Data availability

Data will be made available on request.

Acknowledgments

Authors at Brown University would like to thank for the support from National Science Foundation (NSF) under Award No. 2044631. C.K.,J. at Jeonbuk National University was supported by the National Research Foundation of Korea (NRF) grant funded by the Korea Ministry of Science and ICT (MSIT) (No. 2022R1A2C4002037 and 2022R1A4A3032923). J. L. at Sungkyunkwan University was supported by Korea Environment Industry and Technology Institute (KEITI) grant funded by the Korea Ministry of Environment (MOE) (No. 2019002790003).

Appendix A. Supplementary data

Supplementary data to this article can be found online at https://doi.org/10.1016/j.mtphys.2023.101054.

References

- Y. Balali, S. Stegen, Review of energy storage systems for vehicles based on technology, environmental impacts, and costs, Renew. Sustain. Energy Rev. 135 (2021): 110185, https://doi.org/10.1016/j.rser.2020.110185.
- [2] C.W. Ahn, G. Amarsanaa, S.S. Won, S.A. Chae, D.S. Lee, I.W. Kim, Antiferroelectric thin-film capacitors with high energy-storage densities, low energy losses, and fast discharge times, ACS Appl. Mater. Interfaces 7 (2015) 26381–26386, https://doi. org/10.1021/acsami.5b08786.
- [3] Prateek, V.K. Thakur, R.K. Gupta, Recent progress on ferroelectric polymer-based nanocomposites for high energy density capacitors: synthesis, dielectric properties, and future aspects, Chem. Rev. 116 (2016) 4260–4317, https://doi.org/10.1021/ acs.chemrev.5b00495.
- [4] B. Peng, Q. Zhang, X. Li, T. Sun, H. Fan, S. Ke, M. Ye, Y. Wang, W. Lu, H. Niu, X. Zeng, H. Huang, Large energy storage density and high thermal stability in a highly textured (111)-oriented Pb0.8Ba0.2ZrO3 relaxor thin film with the coexistence of antiferroelectric and ferroelectric phases, ACS Appl. Mater. Interfaces 7 (2015) 13512–13517, https://doi.org/10.1021/acsami.5b02790.
- [5] X. Wang, X. Lu, B. Liu, D. Chen, Y. Tong, G. Shen, Flexible energy-storage devices: design consideration and recent progress, Adv. Mater. 26 (2014) 4763–4782, https://doi.org/10.1002/adma.201400910.
- [6] Q. Li, F.Z. Yao, Y. Liu, G. Zhang, H. Wang, Q. Wang, High-temperature dielectric materials for electrical energy storage, Annu. Rev. Mater. Res. 48 (2018) 219–243, https://doi.org/10.1146/annurey-matsci-070317-124435.
- [7] M.R. Palacín, Recent advances in rechargeable battery materials: a chemist's perspective, Chem. Soc. Rev. 38 (2009) 2565–2575, https://doi.org/10.1039/ b820555b
- [8] S.S. Zhang, Liquid electrolyte lithium/sulfur battery: fundamental chemistry, problems, and solutions, J. Power Sources 231 (2013) 153–162, https://doi.org/ 10.1016/j.ipowsour.2012.12.102.
- [9] M. Armand, J.M. Tarascon, Building better batteries, Nature 451 (2008) 652–657, https://doi.org/10.1038/451652a.
- [10] K. Yao, S. Chen, M. Rahimabady, M.S. Mirshekarloo, S. Yu, F.E.H. Tay, T. Sritharan, L. Lu, Nonlinear dielectric thin films for high-power electric storage with energy density comparable with electrochemical supercapacitors, IEEE Trans. Ultrason. Ferroelectrics Freq. Control 58 (2011) 1968–1974, https://doi.org/ 10.1109/TUFFC.2011.2039.
- [11] Z. Yao, Z. Song, H. Hao, Z. Yu, M. Cao, S. Zhang, M.T. Lanagan, H. Liu, Homogeneous/inhomogeneous-structured dielectrics and their energy-storage performances, Adv. Mater. 29 (2017): 1601727, https://doi.org/10.1002/ adma.201601727.
- [12] I.J. Cohen, J.P. Kelley, D.A. Wetz, J. Heinzel, Evaluation of a hybrid energy storage module for pulsed power applications, IEEE Trans. Plasma Sci. 42 (2014) 2948–2955, https://doi.org/10.1109/TPS.2014.2298369.
- [13] Z. Li, A. Khajepour, J. Song, A comprehensive review of the key technologies for pure electric vehicles, Energy 182 (2019) 824–839, https://doi.org/10.1016/j. energy 2019 06 077
- [14] S.S. Won, M. Kawahara, L. Kuhn, V. Venugopal, J. Kwak, I.W. Kim, A.I. Kingon, S. H. Kim, BiFeO3-doped (K0.5,Na0.5)(Mn0.005,Nb0.995)O3 ferroelectric thin film capacitors for high energy density storage applications, Appl, Phys. Lett. 110 (2017): 152901, https://doi.org/10.1063/1.4980113.
- [15] H. Palneedi, M. Peddigari, G.T. Hwang, D.Y. Jeong, J. Ryu, High-performance dielectric ceramic films for energy storage capacitors: progress and outlook, Adv. Funct. Mater. 28 (2018): 1803665, https://doi.org/10.1002/adfm.201803665.
- [16] E.K. Michael, S. Trolier-McKinsetry, Cubic pyrochlore bismuth zinc niobate thin films for high-temperature dielectric energy storage, J. Am. Ceram. Soc. 98 (2015) 1223–1229, https://doi.org/10.1111/jace.13411.
- [17] E.K. Michael, S. Trolier-McKinstry, Bismuth pyrochlore thin films for dielectric energy storage, J. Appl. Phys. 118 (2015): 054101, https://doi.org/10.1063/ 1.4927738.
- [18] D.P. Cann, C.A. Randall, T.R. Shrout, Investigation of the dielectric properties of bismuth pyrochlores, Solid State Commun. 100 (1996) 529–534, https://doi.org/ 10.1016/0038-1098(96)00012-9.
- [19] A.K. Tagantsev, J. Lu, S. Stemmer, Temperature dependence of the dielectric tunability of pyrochlore bismuth zinc niobate thin films, Appl. Phys. Lett. 86 (2005) 1–3, https://doi.org/10.1063/1.1853533.
- [20] M. Valant, P.K. Davies, Synthesis and dieletric properties of pyrochlore solid solutions in the Bi2O3-ZnO-Nb2O5-TiO2 system, J. Mater. Sci. 34 (1999) 5437–5442, https://doi.org/10.1023/A:1004787706600.
- [21] M.V. Talanov, V.M. Talanov, Structural diversity of ordered pyrochlores, Chem. Mater. 33 (2021) 2706–2725, https://doi.org/10.1021/acs.chemmater.0c04864.
- [22] J.Y. Kim, D.W. Kim, H.S. Jung, K.S. Hong, Influence of strain on the dielectric properties of Bi-Zn-Ti-Nb-O solid solution thin films, J. Eur. Ceram. Soc. 26 (2006) 2161–2164, https://doi.org/10.1016/j.jeurceramsoc.2005.09.075.
- [23] M. Valant, P.K. Davies, Crystal chemistry and dielectric properties of chemically substituted (Bi 1.5 Zn 1.0 Nb 1.5)O 7 and Bi 2 (Zn 23 Nb 43)O 7 pyrochlores, J. Am. Ceram. Soc. 83 (2000) 147–153, https://doi.org/10.1111/j.1151-2916.2000.tb01163.x.
- [24] R.E. Newnham, Electroceramics, Reports Prog. Phys. 52 (1989) 123–156, https://doi.org/10.1088/0034-4885/52/2/001.
- 25] J. Liebault, J. Vallayer, D. Goeuriot, D. Treheux, F. Thevenot, How the trapping of charges can explain the dielectric breakdown performance of alumina ceramics, J. Eur. Ceram. Soc. 21 (2001) 389–397, https://doi.org/10.1016/S0955-2219(00) 00186-2.

- [26] J. Parui, S.B. Krupanidhi, Enhancement of charge and energy storage in sol-gel derived pure and La-modified PbZr O3 thin films, Appl. Phys. Lett. 92 (2008): 192901, https://doi.org/10.1063/1.2928230.
- [27] Y. Zhao, X. Hao, Q. Zhang, Energy-storage properties and electrocaloric effect of Pb (1-3 x/2)LaxZr0.85Ti0.15O 3 antiferroelectric thick films, ACS Appl. Mater. Interfaces 6 (2014) 11633–11639, https://doi.org/10.1021/am502415z.
- [28] X. Hao, J. Zhai, Z. Yue, J. Xu, Phase transformation properties of highly (100)-Oriented PLZST 2/85/12/3 antiferroelectric thin films deposited on Nb-SrTiO3 single-crystal substrates, J. Am. Ceram. Soc. 94 (2011) 2816–2818, https://doi. org/10.1111/j.1551-2916.2011.04736.x.
- [29] S.S. Won, J. Lee, V. Venugopal, D.J. Kim, J. Lee, I.W. Kim, A.I. Kingon, S.H. Kim, Lead-free Mn-doped (K0.5,Na0.5)NbO3 piezoelectric thin films for MEMS-based vibrational energy harvester applications, Appl. Phys. Lett. 108 (2016): 232908, https://doi.org/10.1063/1.4953623.
- [30] F. Ali, X. Liu, D. Zhou, X. Yang, J. Xu, T. Schenk, J. Müller, U. Schroeder, F. Cao, X. Dong, Silicon-doped hafnium oxide anti-ferroelectric thin films for energy storage, J. Appl. Phys. 122 (2017): 144105, https://doi.org/10.1063/1.4989908.
- [31] M.H. Park, H.J. Kim, Y.J. Kim, T. Moon, K. Do Kim, C.S. Hwang, Thin HfxZr1-xO2 films: a new lead-free system for electrostatic supercapacitors with large energy storage density and robust thermal stability, Adv. Energy Mater. 4 (2014): 1400610, https://doi.org/10.1002/aenm.201400610.
- [32] H. Cheng, J. Ouyang, Y.X. Zhang, D. Ascienzo, Y. Li, Y.Y. Zhao, Y. Ren, Demonstration of ultra-high recyclable energy densities in domain-engineered ferroelectric films, Nat. Commun. 8 (2017) 1999, https://doi.org/10.1038/ s41467-017-02040-y.
- [33] B. Peng, Q. Zhang, X. Li, T. Sun, H. Fan, S. Ke, M. Ye, Y. Wang, W. Lu, H. Niu, J. F. Scott, X. Zeng, H. Huang, Giant electric energy density in epitaxial lead-free thin films with coexistence of ferroelectrics and antiferroelectrics, Adv. Electron. Mater. 1 (2015): 1500052, https://doi.org/10.1002/aelm.201500052.
- [34] A.A. Instan, S.P. Pavunny, M.K. Bhattarai, R.S. Katiyar, Ultrahigh capacitive energy storage in highly oriented Ba(ZrxTi1-x)O3 thin films prepared by pulsed laser deposition, Appl. Phys. Lett. 111 (2017): 142903, https://doi.org/10.1063/ 1.4986238.
- [35] X. Hao, A review on the dielectric materials for high energy-storage application, J. Adv. Dielectr. 3 (2013): 1330001, https://doi.org/10.1142/ s2010135x13300016.
- [36] Z. Hu, B. Ma, S. Liu, M. Narayanan, U. Balachandran, Relaxor behavior and energy storage performance of ferroelectric PLZT thin films with different Zr/Ti ratios, Ceram. Int. 40 (2014) 557–562, https://doi.org/10.1016/j.ceramint.2013.05.139.
- [37] Y. Wei, Y. Wen, M. Ou, L. Ke, C. Zeng, Y. Guo, J. Chen, J. He, J. Xu, J. Han, T. Zhai, H. Li, Fusing semiconductor and nonmetal into a high conductive wide-range solid solution alloy for Li-ion batteries, Energy Storage Mater. 42 (2021) 502–512, https://doi.org/10.1016/j.ensm.2021.08.001.
- [38] Q. He, M. Ashuri, Y. Liu, B. Liu, L. Shaw, Silicon microreactor as a fast charge, long cycle life anode with high initial coulombic efficiency synthesized via a scalable method, ACS Appl. Energy Mater. 4 (2021) 4744–4757, https://doi.org/10.1021/ acsaem.1c00351.
- [39] M.S. Javed, A.J. Khan, A. Ahmad, S.H. Siyal, S. Akram, G. Zhao, A.A. Awadh Bahajjaj, M. Ouladsmane, M. Alfakeer, Design and fabrication of bimetallic oxide nanonest-like structure/carbon cloth composite electrode for supercapacitors, Ceram. Int. 47 (2021) 30747–30755, https://doi.org/10.1016/j. ceramint.2021.07.254.
- [40] G. Wang, Z. Lu, Y. Li, L. Li, H. Ji, A. Feteira, D. Zhou, D. Wang, S. Zhang, I. M. Reaney, Electroceramics for high-energy density capacitors: current status and future perspectives, Chem. Rev. 121 (2021) 6124–6172, https://doi.org/10.1021/ acs.chemrev.0c01264.
- [41] P.D. Lomenzo, C.-C. Chung, C. Zhou, J.L. Jones, T. Nishida, Doped Hf 0.5 Zr 0.5 O 2 for high efficiency integrated supercapacitors, Appl. Phys. Lett. 110 (2017): 232904, https://doi.org/10.1063/1.4985297.
 [42] J. Xie, Z. Yao, H. Hao, Y. Xie, Z. Li, H. Liu, M. Cao, A novel lead-free bismuth
- [42] J. Xie, Z. Yao, H. Hao, Y. Xie, Z. Li, H. Liu, M. Cao, A novel lead-free bismuth magnesium titanate thin films for energy storage applications, J. Am. Ceram. Soc. 102 (2019) 3819–3822, https://doi.org/10.1111/jace.16288.
- [43] X. Yang, W. Li, Y. Qiao, Y. Zhang, J. He, W. Fei, High energy-storage density of lead-free (Sr 1–1.5x Bi x)Ti 0.99 Mn 0.01 O 3 thin films induced by Bi 3+ –V Sr dipolar defects, Phys. Chem. Chem. Phys. 21 (2019) 16359–16366, https://doi. org/10.1039/C9CP01368G.
- [44] Z. Tang, J. Ge, H. Ni, B. Lu, X.-G. Tang, S.-G. Lu, M. Tang, J. Gao, High energy-storage density of lead-free BiFeO3 doped Na0.5Bi0.5TiO3-BaTiO3 thin film capacitor with good temperature stability, J. Alloys Compd. 757 (2018) 169–176, https://doi.org/10.1016/j.jallcom.2018.05.072.
- [45] Y. Zhang, W. Li, Y. Qiao, Y. Zhao, Z. Wang, Y. Yu, H. Xia, Z. Li, W. Fei, 0.6ST-0.4NBT thin film with low level Mn doping as a lead-free ferroelectric capacitor with high energy storage performance, Appl. Phys. Lett. 112 (2018): 093902, https://doi.org/10.1063/1.5020679.
- [46] B.B. Yang, M.Y. Guo, D.P. Song, X.W. Tang, R.H. Wei, L. Hu, J. Yang, W.H. Song, J. M. Dai, X.J. Lou, X.B. Zhu, Y.P. Sun, Energy storage properties in BaTiO 3 -Bi 3.25 La 0.75 Ti 3 O 12 thin films, Appl. Phys. Lett. 113 (2018): 183902, https://doi.org/10.1063/15053446
- [47] L. Zhang, B. Yang, J. Yu, Y. Deng, K. Huang, M. Zhang, X. Zhu, Energy storage properties in SrTiO3–Bi3.25La0.75Ti3O12 thin films, J. Alloys Compd. 799 (2019) 66–70, https://doi.org/10.1016/j.jallcom.2019.05.333.
- [48] D.P. Song, J. Yang, B.B. Yang, Y. Wang, L.-Y. Chen, F. Wang, X.B. Zhu, Energy storage in BaBi 4 Ti 4 O 15 thin films with high efficiency, J. Appl. Phys. 125 (2019): 134101, https://doi.org/10.1063/1.5086515.
- [49] B.B. Yang, M.Y. Guo, C.H. Li, D.P. Song, X.W. Tang, R.H. Wei, L. Hu, X.J. Lou, X. B. Zhu, Y.P. Sun, Flexible ultrahigh energy storage density in lead-free

- heterostructure thin-film capacitors, Appl. Phys. Lett. 115 (2019): 243901, https://doi.org/10.1063/1.5128834.
- [50] B. Yang, M. Guo, X. Tang, R. Wei, L. Hu, J. Yang, W. Song, J. Dai, X. Lou, X. Zhu, Y. Sun, Lead-free A 2 Bi 4 Ti 5 O 18 thin film capacitors (A = Ba and Sr) with large energy storage density, high efficiency, and excellent thermal stability, J. Mater. Chem. C 7 (2019) 1888, https://doi.org/10.1039/C8TC05558K. –1895.
- [51] C. Bin, X. Hou, H. Yang, L. Liao, Y. Xie, H. Wei, Y. Liu, X. Chen, J. Wang, Flexible lead-free film capacitor based on BiMg0.5Ti0.5O3-SrTiO3 for high-performance energy storage, Chem. Eng. J. 445 (2022): 136728, https://doi.org/10.1016/j. cei.2022.136728.
- [52] Y. Yao, Y. Li, N. Sun, J. Du, X. Li, L. Zhang, Q. Zhang, X. Hao, High energy-storage performance of BNT-BT-NN ferroelectric thin films prepared by RF magnetron sputtering, J. Alloys Compd. 750 (2018) 228–234, https://doi.org/10.1016/j. iallcom.2018.03.383.
- [53] B.B. Yang, M.Y. Guo, D.P. Song, X.W. Tang, R.H. Wei, L. Hu, J. Yang, W.H. Song, J. M. Dai, X.J. Lou, X.B. Zhu, Y.P. Sun, Bi 3.25 La 0.75 Ti 3 O 12 thin film capacitors for energy storage applications, Appl. Phys. Lett. 111 (2017): 183903, https://doi.org/10.1063/1.4997351.
- [54] S. Wu, P. Chen, J. Zhai, B. Shen, P. Li, F. Li, Enhanced piezoelectricity and energy storage performances of Fe-doped BNT–BKT–ST thin films, Ceram. Int. 44 (2018) 21289–21294, https://doi.org/10.1016/j.ceramint.2018.08.179.
- [55] H. Xu, H. Hao, D. Li, Y. Xie, X. Wang, J. Geng, M. Cao, Z. Yao, H. Liu, Ultrahigh breakdown strength and energy storage properties of xBiMg0.5Zr0.5O3-(1-x) BaZr0.25Ti0.75O3 thin films, Ceram. Int. 48 (2022) 33229–33235, https://doi. org/10.1016/j.ceramint.2022.07.265.
- [56] C. Yang, Q. Yao, J. Qian, Y. Han, J. Chen, Comparative study on energy storage performance of Na.5Bi.5(Ti,W,Ni)O3 thin films with different bismuth contents, Ceram. Int. 44 (2018) 9643–9648, https://doi.org/10.1016/j. ceramint.2018.02.191.
- [57] W. Wang, J. Qian, C. Geng, M. Fan, C. Yang, L. Lu, Z. Cheng, Flexible lead-free Ba0.55r0.5TiO3/0.4BiFeO3-0.6SrTiO3 dielectric film capacitor with high energy storage performance, Nanomaterials 11 (2021) 3065, https://doi.org/10.3390/ nano11113065.
- [58] A. Kursumovic, W.-W. Li, S. Cho, P.J. Curran, D.H.L. Tjhe, J.L. MacManus-Driscoll, Lead-free relaxor thin films with huge energy density and low loss for high temperature applications, Nano Energy 71 (2020): 104536, https://doi.org/ 10.1016/i.nanoen.2020.104536.
- [59] H. Pan, F. Li, Y. Liu, Q. Zhang, M. Wang, S. Lan, Y. Zheng, J. Ma, L. Gu, Y. Shen, P. Yu, S. Zhang, L.-Q. Chen, Y.-H. Lin, C.-W. Nan, Ultrahigh–energy density lead-free dielectric films via polymorphic nanodomain design, Science 365 (2019) 578–582, https://doi.org/10.1126/science.aaw8109.
- [60] C.H. Yang, Q. Yao, J. Qian, Y.J. Han, J. Chen, Growth, microstructure, energy-storage and dielectric performances of chemical-solution NBT-based thin films: effect of sodium nonstoichimometry, Ceram. Int. 44 (2018) 9152–9158, https://doi.org/10.1016/j.ceramint.2018.02.123.
- [61] K. Wang, J. Ouyang, M. Wuttig, Y. Zhao, H. Cheng, Y. Zhang, R. Su, J. Yan, X. Zhong, F. Zeng, Superparaelectric (Ba 0.95, Sr 0.05) (Zr 0.2, Ti 0.8)O 3 ultracapacitors, Adv. Energy Mater. 10 (2020): 2001778, https://doi.org/10.1002/ aepm 202001778
- [62] H. Pan, J. Ma, J. Ma, Q. Zhang, X. Liu, B. Guan, L. Gu, X. Zhang, Y.-J. Zhang, L. Li, Y. Shen, Y.-H. Lin, C.-W. Nan, Giant energy density and high efficiency achieved in bismuth ferrite-based film capacitors via domain engineering, Nat. Commun. 9 (2018) 1813, https://doi.org/10.1038/s41467-018-04189-6.
- [63] Y. Fan, Z. Zhou, Y. Chen, W. Huang, X. Dong, A novel lead-free and high-performance barium strontium titanate-based thin film capacitor with ultrahigh energy storage density and giant power density, J. Mater. Chem. C 8 (2020) 50–57, https://doi.org/10.1039/C9TC04036F.
- [64] N. Sun, Y. Li, Q. Zhang, X. Hao, Giant energy-storage density and high efficiency achieved in (Bi 0.5 Na 0.5)TiO 3 –Bi(Ni 0.5 Zr 0.5)O 3 thick films with polar nanoregions, J. Mater. Chem. C 6 (2018) 10693–10703, https://doi.org/10.1039/ C8TC03481H.
- [65] B. Song, S. Wu, F. Li, P. Chen, B. Shen, J. Zhai, Excellent energy storage density and charge–discharge performance of a novel Bi 0.2 Sr 0.7 TiO 3 –BiFeO 3 thin film, J. Mater. Chem. C 7 (2019) 10891–10900, https://doi.org/10.1039/C9TC03032H.
- [66] J. Wang, Y. Li, N. Sun, Q. Zhang, L. Zhang, X. Hao, X. Chou, Effects of Fe3+ doping on electrical properties and energy-storage performances of the (Na0.85K0.15) 0.5Bi0.5TiO3 thick films prepared by sol-gel method, J. Alloys Compd. 727 (2017) 596–602, https://doi.org/10.1016/j.jallcom.2017.08.169.
- [67] J. Wang, N. Sun, Y. Li, Q. Zhang, X. Hao, X. Chou, Effects of Mn doping on dielectric properties and energy-storage performance of Na0.5Bi0.5TiO3 thick films, Ceram. Int. 43 (2017) 7804–7809, https://doi.org/10.1016/j. ceramint 2017 03 094
- [68] Z. Xu, X. Hao, S. An, Dielectric properties and energy-storage performance of (Na0.5Bi0.5)TiO3-SrTiO3 thick films derived from polyvinylpyrrolidone-modified chemical solution, J. Alloys Compd. 639 (2015) 387–392, https://doi.org/ 10.1016/j.jallcom.2015.03.133.
- [69] Z. Liang, M. Liu, C. Ma, L. Shen, L. Lu, C.-L. Jia, High-performance BaZr 0.35 Ti 0.65 O 3 thin film capacitors with ultrahigh energy storage density and excellent

- thermal stability, J. Mater. Chem. A. 6 (2018) 12291–12297, https://doi.org/
- [70] H. Pan, S. Lan, S. Xu, Q. Zhang, H. Yao, Y. Liu, F. Meng, E.-J. Guo, L. Gu, D. Yi, X. Renshaw Wang, H. Huang, J.L. MacManus-Driscoll, L.-Q. Chen, K.-J. Jin, C.-W. Nan, Y.-H. Lin, Ultrahigh energy storage in superparaelectric relaxor
- ferroelectrics, Science 80– (374) (2021) 100–104, https://doi.org/10.1126/science.abi7687.
- [71] M. Peddigari, H. Palneedi, G.-T. Hwang, K.W. Lim, G.-Y. Kim, D.-Y. Jeong, J. Ryu, Boosting the recoverable energy density of lead-free ferroelectric ceramic thick films through artificially induced quasi-relaxor behavior, ACS Appl. Mater. Interfaces 10 (2018) 20720–20727, https://doi.org/10.1021/acsami.8b05347.